Low-frequency dynamics of separated boundary-layer

Stefania Cherubini [1,2]**, Jean-Christophe Robinet** [1] **& Pietro De Palma** [2]

[1] *Laboratoire DYNFLUID - Arts & Métiers ParisTech - 151 Bd. de l'Hôpital - 75013 Paris - France,* [2] *DIMeG, CEMeC, Politecnico di Bari - Via Re David 200 - 70125 Bari - Italie*
Jean-Christophe.Robinet@paris.ensam.fr

Résumé :

Dans ce papier nous nous intéressons à la dynamique transitoire et asymptotique d'une couche limite de plaque plane fortement décollée. Seul le régime supercritique (linéairement globalement instable) est abordé. Les effets de la non-normalité de l'opérateur linéarisé sont étudiés en détail ainsi que l'influence des non-linéarités pour des perturbations d'amplitude finie. L'étude de la dynamique est d'une part réalisée par la résolution d'un problème aux valeurs propres de grande dimension et la résolution des équations de Navier-Stokes directes. Les analyses de stabilité globale ainsi que les simulations numériques initialisées par des perturbations d'amplitude croissante montrent que l'écoulement est globalement instable et se comporte comme un oscillateur engendrant des oscillations auto-entretenues de basses fréquences à temps longs.

Abstract :

The effects of non-normality and non-linearity of the two-dimensional differential Navier-Stokes operator on the dynamics of a large laminar separation bubble over a flat plate have been studied in a slightly supercritical conditions. The global eigenvalue analysis together with direct numerical simulations have been employed in order to investigate the linear and non-linear stability of the flow. For supercritical conditions, the non-normality of the modes has been found to generate low-frequency oscillations (flapping) at large times.

Mots-clefs :

global eigenvalue analysis, direct numerical simulation, optimal response, flapping frequency

1 Introduction

In many engineering applications the boundary layer undergoes separation and reattachment, thus forming recirculation bubbles whose stability and control may be crucial for the performance of the device under consideration. This may happen, for example, over the surface of turbomachinery blades or of airplane wings. Separation may be triggered by the geometry of the body or by the adverse pressure gradient. In both cases the aerodynamic load may be strongly affected by the behavior of the bubble which changes its characteristics depending on the operating conditions. Often, the presence of a bubble is associated with a laminar-turbulent transition of the boundary layer since flow separation occurs in the laminar part of the bubble and, after transition, the flow reattaches. Such a transition is governed by the amplification of flow perturbations which may be due either to a linear process based on transient growth or to a non-linear one in the presence of high free-stream disturbance levels (bypass transition) [1].

In [2], a thorough analysis is provided of the different transition mechanisms with respect to two and three-dimensional initial perturbations, showing that several transition scenarios are possible and that, when small amplitudes perturbation are considered, two-dimensional disturbances are the most amplified ones. On the other hand, laminar separation bubbles show a strong two-dimensional instability mechanism known as "flapping" [3] and a high sensitivity to external noise [4] whose basic features are still not fully understood. In particular, the following issues need to be investigated : i) the role of the convective Kelvin–Helmholtz instability of the shear layer along the separation streamline with respect to the flapping phenomenon ; ii) the mechanism of transition from convective to global instability ; iii) the influence of topological flow changes on the stability behavior (see [5] for a complete review).

The present work provides a stability analysis of the two-dimensional flow over a flat plate with a separation bubble induced by a suction-and-blowing velocity profile. The aim of this paper is to describe the linear and non-linear dynamics of a large separation bubble at low Reynolds numbers due to the non-orthogonality of the eigenvectors of the differential operator, leading to self-sustained oscillations and large transient amplifications of the initial disturbances. Therefore, a two-dimensional direct numerical simulation (DNS) is employed as a complementary tool with respect to the global eigenvalue analysis for validating the results obtained by the eigenvalue analysis in the linear case and for studying the non-linear dynamics of separated flows.

2 Governing equation and boundary conditions

The two-dimensional incompressible flow over a flat plate has been computed by solving the Navier–Stokes equations,

$$\begin{aligned} \mathbf{u}_t + (\mathbf{u}\cdot\bigtriangledown)\mathbf{u} &= -\bigtriangledown p + \frac{1}{Re}\bigtriangledown^2\mathbf{u}, \\ \bigtriangledown\cdot\mathbf{u} &= 0, \end{aligned} \tag{1}$$

where $\mathbf{u} = (u, v)^T$ is the velocity vector and p is the pressure. Dimensionless variables are defined with respect to the inflow displacement thickness, δ^*, and to the freestream velocity, U_∞, so that the Reynolds number is equal to $Re = U_\infty\delta^*/\nu$, where ν is the kinematic viscosity coefficient. A rectangular computational domain with dimensions $L_x = 420$, $L_y = 30$ is employed, x and y being the streamwise and wall-normal directions, respectively. At inlet points, placed at $x = 65$ displacement thickness units from the leading edge of the bottom wall, a Blasius boundary-layer profile is imposed for both the streamwise, u, and wall-normal, v, components of the velocity vector, whereas, at outlet points, a standard convective condition is employed. At the bottom wall, the no-slip boundary condition is prescribed. Finally, at the upper-boundary points, a suction-and-blowing profile for the v-component of the velocity [6] is imposed, and the vorticity is set to zero.

3 Numerical methods

The Navier–Stokes equations are integrated by a fractional step method using a staggered grid [7]. The viscous terms are discretized in time using an implicit Crank–Nicholson scheme, whereas an explicit third-order-accurate Runge–Kutta scheme is employed for the non-linear terms. A second-order-accurate centered space discretization has been used for the linear terms, whereas, for the present calculations, a sixth-order-accurate space discretization has been im-

plemented for the non-linear terms, based on a combined compact scheme for non-uniform grids [8]. All numerical simulations provided in the present work have been performed discretizing the computational domain by a 501×150 Cartesian grid stretched in the wall-normal direction, the height of the first cell close to the wall being equal to 0.1.
The above DNS method has been used to perform all the non-linear simulations, and to compute the base flow for the global stability analysis at subcritical Reynolds number. However, using the DNS, the residual cannot be reduced to machine zero when computing the base flow at supercritical as well as at slightly subcritical Reynolds numbers since some frequencies present in the numerical noise are highly amplified. In these cases, several approaches may be employed to compute the base flow, based on filtering techniques or on continuation methods. Here, a time-stepping continuation method has been employed. Therefore, following the procedure proposed in [9], the DNS method has been combined with a Newton steady-state solver. The Newton method has been used for the computation of the base flows at supercritical Reynolds numbers and at slightly subcritical ones, the iterations have been stopped when a residual level of 10^{-12} has been achieved.

4 Linearized dynamics

Once the base flows have been computed for several values of the Reynolds number, their global stability is studied by means of a perturbative technique, namely, by considering the instantaneous variables, $\mathbf{q}$, as a superposition of the base flow and of the perturbation $\mathbf{q}' = (u', v', p')^T$. Such a perturbation is decomposed in temporal modes as :

$$\mathbf{q}'(x, y, t) = \sum_{k=1}^{N_t} \kappa_k^0 \, \hat{\mathbf{q}}_k(x, y) \exp\left(-i\omega_k t\right), \tag{2}$$

where N_t is the total number of modes, $\hat{\mathbf{q}}_k$ are the eigenvectors, ω_k are the eigenmodes (complex frequencies), and κ_k^0 represents the initial energy of each mode. A substitution of such a decomposition in equation (1) and a successive linearization lead to the following eigenvalue problem

$$\left(\mathbf{A} - i\omega_k \mathbf{B}\right) \hat{\mathbf{q}}_k = \mathbf{0}, \quad k = 1, \ldots, N_t. \tag{3}$$

The problem (3) is discretized with a Chebyshev/Chebyshev collocation spectral method employing $N_t = 850$ modes, and is solved with a shift-and-invert Arnoldi algorithm using the ARPACK library [10], the residual being reduced to 10^{-12}. At upper and inlet boundaries, a zero perturbation condition is imposed, whereas at the outflow, being the flow locally unstable, a Robin condition based on the approximation of the local dispersion relation is prescribed [11, 12]. Concerning the subcritical flow computations, the modes are discretized using $N_x = 250$ collocation points in the x-direction and $N_y = 48$ collocation points in the y-direction.
However, although the modes have been found asymptotically unstable, they are likely to interact leading to a transient amplification of the perturbations, due to the non-orthogonality of the corresponding eigenvectors. With the aim of measuring such an amplification, let us define the energy of the perturbations at time t as :

$$E\left(t\right) = \frac{1}{2} \int_0^{L_x} \int_0^{L_y} \left(u'^2 + v'^2\right) \, dxdy. \tag{4}$$

Furthermore, the maximum energy gain, $G(t)$, obtainable at time t over all possible initial conditions, $\mathbf{u}'_0$, is defined as :

$$G(t) = \max_{\mathbf{u}'_0 \neq 0} \frac{E(t)}{E(0)}. \tag{5}$$

By decomposing the perturbation into the eigenmode basis (2), it is possible to rewrite equation (5) in the following form :

$$G(t) = ||\mathbf{F} \exp(-it\mathbf{\Lambda})\mathbf{F}^{-1}||_2^2, \tag{6}$$

where $\mathbf{\Lambda}$ is the diagonal matrix of the eigenvalues, ω_k, and $\mathbf{F}$ is the Cholesky factor of the energy matrix $\mathbf{M}$ of components,

$$M_{ij} = \int\int (\hat{u}_i^* \hat{u}_j + \hat{v}_i^* \hat{v}_j)\, dxdy, \quad i,j = 1,\ldots,N_t, \tag{7}$$

where the superscript "*" denotes the complex-conjugate. Finally, the maximum amplification at time t and the corresponding optimal initial condition, $\mathbf{u}'_0$, are computed by a singular value decomposition of the matrix $\mathbf{F} \exp(-it\mathbf{\Lambda})\mathbf{F}^{-1}$ [1].

5 Unstable dynamics : the origin of unsteadiness and the flapping frequency

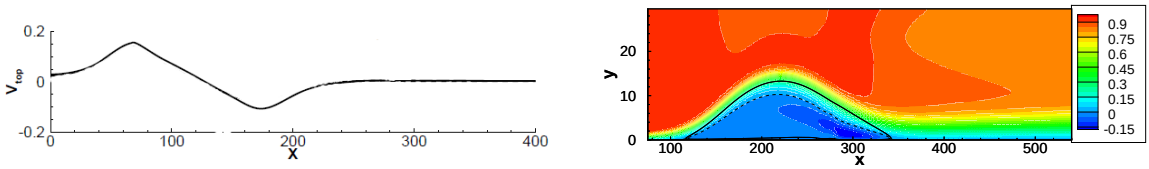

(a) (b)

FIGURE 1 – (a) : Suction-and-blowing profiles imposed at the upper boundary for the v-component of the velocity. (b) : Streamwise velocity contours of the base flow at Reynolds number $Re = 225$. The solid line is the separation streamline, whereas the dashed line represents the $u = 0$ contour.

The supercritical dynamics of the flow has been investigated by performing the global eigenvalue analysis with increasing Reynolds numbers. Transition has been found to occur at $Re = 225$. Figure 1 shows the corresponding streamwise velocity contours of the base flow and the associated suction velocity profile. The structure of the spectrum at such a Reynolds number is provided in Figure 2. The spectrum is marginally unstable, since there are seven slightly unstable modes placed on the convective branch, their eigenvectors being reminiscent of

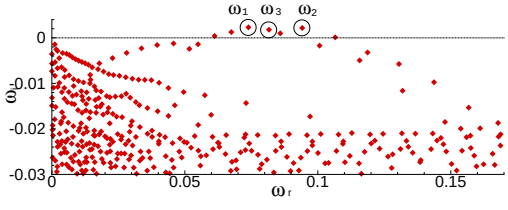

FIGURE 2 – Eigenvalue spectrum for the flow at $Re = 225$ with $N_x = 270$ and $N_y = 50$ grid points. The modes labelled ω_1, ω_2 and ω_3 are the most unstable ones.

the TS waves. The linear energy growth has been studied using the global eigenvalue analysis for increasing Reynolds numbers. The behavior of the corresponding energy-gain curves, reported in Figure 3, shows that : i) the first peak value increases linearly with respect to Re ; ii) the time at which the first peak occurs increases linearly with respect to Re. Recalling that the transient energy growth in the considered case is due to the Kelvin-Helmholtz amplification along the separation streamline, one can assume that the increase of $G(t)$ is due to the increase of the size of the bubble with the Reynolds number. In the slightly unstable case ($Re = 225$), a linear energy gain equal about to 10^{12} has been found, as shown by the top curve in Figure 3. In order to further investigate the linear unstable dynamics of an initial perturbation, the evolution of the optimal perturbation at $Re = 225$ has been studied. As shown in Figure 4, the perturbation is initially convected downstream by the mean flow as a localized wave packet. A second wave packet is generated due to the amplification of the disturbances carried back by the recirculation bubble. Such a disturbance shedding cycle is not due to an absolute instability of the velocity profiles within the bubble, as assessed by a local eigenvalue analysis, but to the global characteristics of the flow. The generation of wave packets by the cyclic transfer of energy from the upstream part to the downstream part of the bubble and vice-versa seems to be a feature of the stability dynamics of such a separated flow.

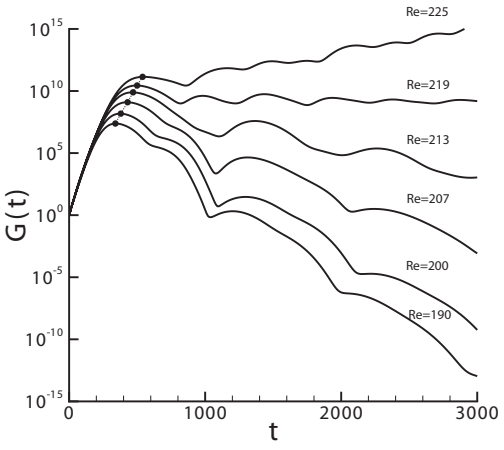

FIGURE 3 – Optimal energy gain curves obtained by the global eigenvalue analysis with $N_t = 400$ modes.

Focusing now on the asymptotic behavior of the flow at different Reynolds numbers, one can observe in Figure 3 that each energy gain curve is affected by a modulation. Such a modulation, also named beating or flapping frequency, is a well-known feature of separated flows [13, 14, 3]. Such a phenomenon is due to the interaction of the most unstable modes of the spectrum. Since such modes are associated to similar eigenvectors, they are able to interact resulting in the low frequency modulation observed for the energy gain curve. For instance, at $Re = 225$, the first frequency (labeled as I) corresponds to the low-frequency beating found in the previous case, having a period of about $T \approx 850$. The second frequency (labeled as II) is slightly higher than the first one, having a period of about $T \approx 300$. Indeed, by looking at the spectrum at $Re = 225$, provided in Figure 2, one can notice that the three most unstable modes have very similar amplification rate, leading to cancelation as in the stable case. Since their real parts differ of about $\delta\omega_{r_I} = \omega_{r_3} - \omega_{r_1} \approx 0.0075$, and $\delta\omega_{r_{II}} = \omega_{r_2} - \omega_{r_3} \approx 0.02$, they result respectively in two wave packets of period $T_I = 2\pi/\delta\omega_{r_I} \approx 850$ and $T_{II} = 2\pi/\delta\omega_{r_{II}} \approx 300$ and which corresponds to the modulation shown in Figure 3 by the energy gain curve. It is worth to notice that, due to the linearity of the global eigenvalue analysis, for large values of t the beating induced by the two most unstable modes (frequency II) dominates the other one.

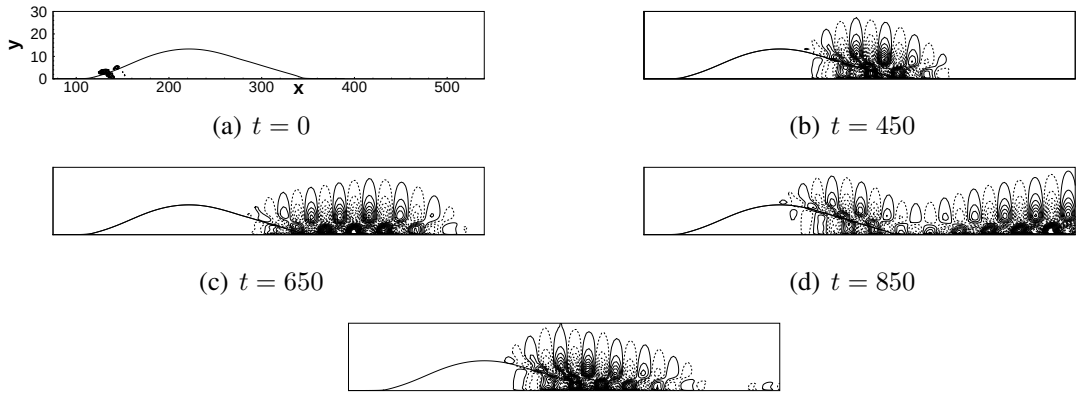

(a) $t = 0$ (b) $t = 450$

(c) $t = 650$ (d) $t = 850$

(e) $t = 1050$

FIGURE 4 – Streamwise perturbation velocity contours of the optimal perturbation obtained by the global eigenvalue analysis for $Re = 225$. Solid-line contours indicate positive velocities ; dashed-line ones are associated with negative velocities.

The physical mechanism governing the beating phenomenon has been studied by performing several numerical simulations with increasing Reynolds numbers. DNS predicts transition at $Re = 230$, which is close but not exactly equal to the critical Reynolds number obtained by the linear analysis, namely $Re = 225$. The time evolution of the energy gain has been computed by DNS, it is possible to observe that two modulations affect the energy gain curve after the transient has passed, with periods $T_I \approx 900$ and $T_{II} \approx 350$. Such results are in good agreement with the ones found by using the global eigenvalue analysis. The power density spectrum of the streamwise velocity perturbation at a point within the bubble ($x = 339$, $y = 1.4$) has been computed, two frequency ranges where the energy is mostly located are found. The higher frequency range corresponds to TS waves, since the pulsations in the range $0.06 < \omega_r < 0.12$ correspond to the globally unstable modes of Figure 2. Moreover, in the low-frequency region it is possible to recover three leading pulsations which are close to the flapping frequencies I and II and to their difference, respectively ($\omega_I \approx 0.005$, $\omega_{II} \approx 0.014$ and $\omega_{III} = \omega_{II} - \omega_I \approx 0.009$). Figure 5 provides a summary of these results.

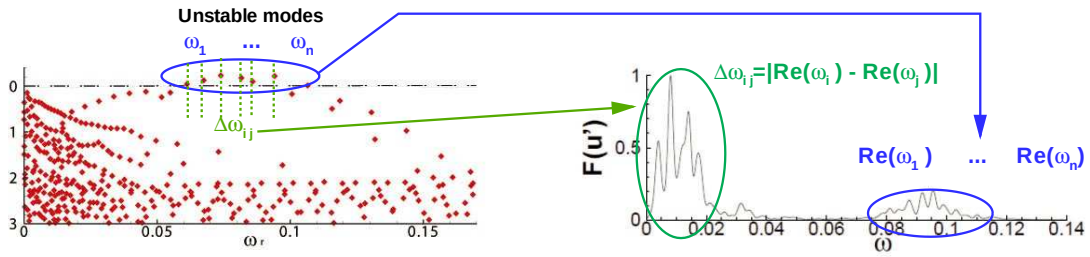

FIGURE 5 – Schematic summary showing the dynamics of a flat plate separated boundary layer.

6 Conclusion

The transient and asymptotical dynamics of a large separation bubble over a flat plate has been studied. Two numerical tools have been employed, namely, the global eigenvalue analysis and the direct numerical simulation at slightly supercritical Reynolds numbers. Linear eigenvalue analysis as well as numerical simulations with weakly non-linear perturbations have shown that the non-normality of convective modes of the Navier–Stokes operator allows the separated boundary-layer flow to develop a self-sustained low frequency dynamics if the Reynolds number is sufficiently high. In fact, due to the superposition of two convective non-normal modes, a low-frequency oscillation, known as flapping frequency, appears. A possible explanation of such a behavior has been provided, in which it is assumed that the oscillations are due to the interaction of the main wave packet with the perturbations carried upstream by the backflow inside the bubble. Preliminary DNS results show that the flapping frequencies are recovered also in a three-dimensional configuration, and that their values are close to the ones here obtained for the two-dimensional case.

Références

[1] P. Schmid and D. Henningson. *Stability and transition in shear fows*. Springer, 2001.

[2] U. Rist and U. Maucher. Direct numerical simulation of 2-D and 3-D instability waves in a laminar separation bubble. *AGARD-CP-551*, April 1994.

[3] U. Ehrenstein and F. Gallaire. Global low-frequency oscillations in a separating boundary-layer flow. *J. Fluid Mech.*, 614 :315–327, 2008.

[4] F. Alizard, S. Cherubini, and J. Ch. Robinet. Sensitivity and optimal forcing response in separated boundary layer flows. *Physics of Fluids*, 21 :064108, 2009.

[5] A. V. Dovgal, V. V. Kozlov, and A. Michalke. Laminar boundary layer separation : instability and associated phenomena. *Prog. Aerospace Sci.*, 30(1) :61–94, 1994.

[6] Y. Na and P. Moin. The structure of wall-pressure fluctuations in turbulent boundary layers with adverse pressure gradient and separation. *J. Fluid Mech.*, 377 :347–373, 1998.

[7] R. Verzicco and P. Orlandi. A finite-difference scheme for the three-dimensional incompressible flows in cylindrical coordinates. *J. Comp. Phys.*, 123(2) :402–414, 1996.

[8] P. Chu and C. Fan. A three point sixth-order non uniform combined compact difference scheme. *J. Comp. Phys.*, 148(2) :663–674, 1999.

[9] L. S. Tuckerman and D. Barkley. Bifurcation analysis for Timesteppers. *Numerical Methods for Bifurcation Problems and Large-Scale Dynamical Systems*, 119(543–466), 2000.

[10] R. Lehoucq, D. Sorensen, and C. Yang. *ARPACK Users' Guide : Solution of Large Scale Eigenvalue Problems with Implicitly Restarted Arnoldi Methods*. SIAM, 1997.

[11] U. Ehrenstein and F. Gallaire. On two dimensional temporal modes in spatially evolving open flows : the flat-plate boundary layer. *J. Fluid Mech.*, 536 :209–218, 2005.

[12] F. Alizard and J.-C. Robinet. Spatially convective global modes in a boundary layer. *Phys. Fluids*, 19(114105), 2007.

[13] E. Akervik, J. Hoepffner, U. Ehrenstein, and D. S. Henningson. Optimal growth, model reduction and control in a separated boundary-layer flow using global eigenmodes. *J. Fluid Mech.*, 579 :305–314, 2007.

[14] F. Alizard and J.-C. Robinet. Convective and Global Instabilities in Separated Flows. *6th ICIAM*, 2007.